

Hot Hydrogen Climates near the inner edge of the Habitable Zone

Daniel D.B. Koll¹ and Timothy W. Cronin¹

¹*Department of Earth, Atmospheric and Planetary Sciences, Massachusetts Institute of Technology, Cambridge, MA, 20139.*

Abstract

Young terrestrial planets can capture or outgas hydrogen-rich atmospheres with tens to hundreds of bars of H₂, which persist for 100 Myrs or longer. Although the earliest habitable conditions on Earth and terrestrial exoplanets could thus arise while the atmosphere is still dominated by H₂, the climatic effects of H₂ remain poorly understood. Previous work showed that H₂ induces strong greenhouse warming at the outer edge of the habitable zone. Here we use a 1D radiative-convective model to show that H₂ also leads to strong warming near the inner edge of the habitable zone. Unlike H₂'s greenhouse warming at the outer edge, however, its effect near the inner edge is driven by thermodynamics: H₂'s large thermal scale height allows the atmosphere to store more water vapor than either a pure-H₂O atmosphere or an atmosphere with a heavy background gas, such as N₂ or CO₂, thereby amplifying the greenhouse effect of H₂O. Using idealized grey calculations, we then present a general argument for how different background gases affect the inner edge of the habitable zone. H₂ stands out for its ability to induce novel 'Soufflé' climates, which further support its warming effect. Our results show that if the earliest conditions on a planet near the inner edge of the habitable zone were H₂-rich, they were likely also hot: 1 bar of H₂ is sufficient to raise surface temperatures above 340 K, and 50 bar of H₂ are sufficient to raise surface temperatures above 450 K.

Key words: planetary atmospheres – astrobiology – exoplanets

1. Introduction

Hydrogen plays an important role in the early stages of terrestrial planet evolution. Planets that form inside a nebular disk are likely to gravitationally capture a primordial H₂ atmosphere (Rafikov 2006; Pierrehumbert & Gaidos 2011). Even after the disk disperses, planets can outgas H₂ during the solidification of the planet's magma ocean (Elkins-Tanton & Seager 2008; Schaefer & Fegley 2010), or can form H₂ through the oxidation of iron-rich impactors during the giant impact phase (Genda et al. 2017). The amount of H₂ generated varies with formation mechanism but can be substantial, ranging from several to more than 1000 bars (Pierrehumbert & Gaidos 2011; Elkins-Tanton & Seager 2008; Genda et al. 2017).

H₂ eventually dissipates because its low molecular weight allows it to escape to space. In the meantime, however, it can shape a planet's earliest surface conditions. To order of magnitude, we estimate that it takes ~ 100 Myr for a young Earth-like planet around a Sun-like star to lose 100 bars of H₂ to space (see Appendix A). This timescale becomes longer if H₂ is produced or outgassed later, due to the rapid decrease over time in the XUV output of young Sun-like stars. Our estimate agrees with the results of Genda et al. (2017), who argued that early Earth could have had a ~ 70 bar H₂ atmo-

sphere which gradually escaped over 200 Myr, produced by the oxidation of fragments from a giant impact.

These timescales are longer than the 1 – 10 Myr needed to solidify a magma ocean and condense a steam atmosphere (Hamano et al. 2013; Lebrun et al. 2013). They are also long enough to shape prebiotic chemistry and, potentially, for an early biosphere to develop (Lazcano & Miller 1994; Bell et al. 2015; Betts et al. 2018). Some terrestrial planets, including ancient Earth, could therefore undergo an early habitable phase with liquid water oceans underneath a H₂ atmosphere. What would such a climate be like?

The habitable zone has conventionally only been studied for an atmosphere dominated by high mean-molecular-weight (MMW) background gases, in particular N₂ and CO₂ (e.g. Kasting et al. 1993; Kopparapu et al. 2013). There are relatively few studies that have considered the habitability of H₂-rich planets, and these studies either focused on thick H₂ atmospheres at the outer edge of the habitable zone or atmospheres with relatively small amounts of H₂. In both cases, hydrogen can have a significant effect on climate. Thick H₂ envelopes, with tens of bars of H₂, generate a strong greenhouse effect via H₂-H₂ collision-induced absorption that can allow planets to remain habitable far beyond the outer edge of the conventional N₂-CO₂ habitable zone (Stevenson 1999; Pierrehumbert & Gaidos 2011; Wordsworth 2012). Similarly, even small amounts of H₂, on the order of 1-30% molar fraction, can induce greenhouse warming via H₂-N₂ or H₂-CO₂ collision-induced absorption. H₂ could thus also help

resolve the Faint Young Sun problem on early Earth and early Mars, and could expand the outer edge of the habitable zone (Wordsworth & Pierrehumbert 2013; Ramirez et al. 2014; Batalha et al. 2015; Ramirez & Kaltenegger 2017).

Less attention has been paid to how a transient H_2 atmosphere, with 1 or more bars of H_2 , would affect a planet’s climate closer to the inner edge of the habitable zone, which we consider in this work. Unlike at the outer edge, where H_2 ’s radiative effect dominates, the interaction between water vapor and the H_2 background becomes increasingly important near the inner edge, which we define as roughly the region where the incident stellar flux, or stellar constant, exceeds 1000 W m^{-2} ($\sim 70\%$ of the flux received by Earth today). We explore these interactions with a 1D radiative-convective model that represents a planet orbiting a Sun-like star. To relate our results to conventional N_2 - CO_2 habitable zone calculations, we consider both high MMW and H_2 -rich atmospheres (the model is described in Section 2). Our results fall into two categories. First, we show that H_2 has a strong warming effect near the inner edge. This effect is independent of H_2 ’s greenhouse effect and instead arises from hydrogen’s thermodynamic properties (Section 3). Second, we present a general consideration for how a planet’s background gases affect its climate, with a particular focus on the approach to the runaway greenhouse. We show that a habitable planet has distinct climate feedbacks with H_2 versus high-MMW backgrounds, and that these feedbacks give rise to novel climate states in H_2 -rich atmospheres which further support H_2 ’s warming effect (Section 4). Finally, we discuss our findings and its implications for the origin of life in the early Solar System and around other stars (Section 5).

2. Methods

We the Python line-by-line RADIation model for planetary atmosphereS (PyRADS), which is a 1D model representing an atmosphere in radiative-convective equilibrium. We have validated PyRADS against other line-by-line calculations in the longwave (Koll & Cronin 2018), as well as the shortwave (Appendix B). The model code is open source and freely available on github¹.

The atmosphere is composed of a dry background gas (e.g., N_2 or H_2) plus condensing water vapor. The amount of atmospheric water vapor increases rapidly with temperature following the Clausius-Clapeyron relation, so all atmospheres become steam-dominated at high temperatures. For example, the saturation vapor pressure of water is $\sim 6 \times 10^{-3}$ bar at the triple point (273 K), whereas it is one bar at the boiling point (373 K). A planet with 1 bar of background N_2 at a surface temperature of 273 K therefore has an atmosphere that is largely made of N_2 , whereas at 373 K the total surface pressure rises to 2 bar and the air near the ground contains as many H_2O molecules as N_2 molecules.

To compute convective temperature profiles we use the general moist adiabat, which is valid for both a dry atmosphere and a steam-dominated atmosphere (Ding & Pierre-

humbert 2016). All thermodynamic constants are taken from Pierrehumbert (2010). We choose a variable vertical resolution to ensure that we resolve the upper atmosphere in the runaway limit, yet also have good resolution near the surface at intermediate surface temperatures.

For the radiative transfer we perform two separate calculations in the longwave and shortwave. Our longwave calculations cover the spectrum up to $5,000 \text{ cm}^{-1}$ ($2 \mu\text{m}$) with a spectral resolution of 0.01 cm^{-1} . In the shortwave we cover the spectrum between $1,000$ and $110,000 \text{ cm}^{-1}$ (0.09 - $10 \mu\text{m}$) with a spectral resolution of 0.01 cm^{-1} up to $30,000 \text{ cm}^{-1}$ and a resolution of 10 cm^{-1} at higher wavenumbers (see below). We assume a Sun-like host star, with a solar spectrum taken from the VPL database (Segura et al. 2003), and a surface albedo of 0.12. To solve the shortwave radiative transfer we use DISORT (Stamnes et al. 1988), implemented via PyDISORT². We run DISORT at line-by-line resolution using 4 angular streams. Sensitivity tests indicate that our results are essentially identical if we use more angular streams.

To compute opacities we use a combination of H_2O lines from HITRAN2016 (Gordon et al. 2017) and the more comprehensive ExoMol BT2 line list (Barber et al. 2006). At the temperatures we are considering, the choice of line list only has a minor impact on longwave fluxes because HITRAN2016 already contains most strong absorption lines in the infrared. In contrast, shortwave fluxes are sensitive to the choice of line list because HITRAN2016 does not cover the UV even though the near and middle UV contains a moderate fraction of the incoming stellar flux ($\sim 8\%$ for a Sun-like star). As a compromise between computational tractability and complete spectral coverage we adopt HITRAN2016 lines below $15,000 \text{ cm}^{-1}$ and BT2 lines between $15,000 \text{ cm}^{-1}$ and $30,000 \text{ cm}^{-1}$. Similarly, for computational tractability in our CO_2 calculations we use the HITRAN2016 line list. We use a Lorenz line shape throughout instead of a Voigt line shape. This approximation means we do not resolve line cores, but the resulting impact on OLR is small (Koll & Cronin 2018).

H_2O line broadening could behave differently in a N_2 versus a H_2 atmosphere. To explore this possibility we compared line widths for H_2O -air broadening (Voronin et al. 2010) with line widths for H_2O - H_2 broadening (Barton et al. 2017). Despite our expectation that collisional line width should scale with intermolecular velocity (Pierrehumbert 2010), and hence with the inverse square root of the broadening gas’s molecular mass, H_2O line widths are roughly the same for H_2 and N_2 broadening. In both cases the widths of the strongest lines are about $0.1 \text{ cm}^{-1} \text{ atm}^{-1}$. Although this invariance might be particular to H_2 and N_2 , because line widths for H_2O -He collisions are noticeably smaller (Barton et al. 2017), we use H_2O -air broadening parameters for both N_2 and H_2 .

In addition to line opacities we include several other opacity sources. We compute H_2O - H_2O and H_2O -foreign collision-induced absorption (CIA) using the semi-empirical MTCKD continuum model (Mlawer et al. 2012). For H_2 -

¹ github.com/ddbkoll/PyRADS-shortwave

² github.com/chanGimeno/pyDISORT

H₂ CIA we use data from HITRAN. We are not aware of any H₂O-H₂ CIA data, so we use H₂O-N₂ CIA in both our N₂ and our H₂ calculations. Our use of H₂O-N₂ data to mimic H₂O-H₂ CIA could induce errors but is reasonable given the lack of laboratory measurements: N₂ and H₂ are both homonuclear diatomics, so to first order one might expect them to similarly interact with the H₂O molecule and its electric field moments. For CO₂-CO₂ and CO₂-foreign CIA we use data from Pierrehumbert (2010). For Rayleigh scattering we use the N₂ and H₂O scattering cross-sections from Goldblatt et al. (2013), the H₂ scattering cross-sections from Dalgarno & Williams (1962), and the CO₂ scattering cross-sections from Pierrehumbert (2010). We parameterize absorption in the UV by setting the absorption cross-section of H₂O at frequencies higher than 50,000 cm⁻¹ (0.2 μm) equal to a representative value based on the MPI-Mainz Atlas, $\kappa_{UV} \approx 10^{-18} \text{ cm}^2 \text{ molec}^{-1} = 3 \times 10^3 \text{ m}^2 \text{ kg}^{-1}$.

Consistent with our use of a 1D model we do not include effects that are determined by 3D dynamics, such as clouds or changes in relative humidity. Instead we assume clear-sky profiles and a relative humidity of unity. We also assume an all-adiabat atmosphere in which convection reaches to the top of the atmosphere, and ignore the stratosphere. We discuss the impact of these modeling assumptions in Section 5.

For our analytical results in Section 4 we note that the definition of optical thickness often includes a implicit average cosine of the zenith angle, $\overline{\cos \theta}$, which accounts for the angular distribution of longwave radiation (Pierrehumbert 2010). Our numerical calculations use $\overline{\cos \theta} = 3/5$. To reproduce our analytical values, optical thickness τ along a vertical path should be divided by $\overline{\cos \theta}$.

Below we will present our results in terms of the planet's surface temperature T_s as a function of incoming stellar flux (Figure 1). To present our results in this way we first run our model across a large grid of surface temperatures. The model outputs albedo α and OLR, which then allows us to infer the stellar flux L_* that would be required to maintain a given surface temperature via planetary energy balance, $L_* = 4\text{OLR}(T_s)/(1 - \alpha(T_s))$. We refer to a climate state as stable if warming increases the planet's OLR more than it increases the planet's absorbed shortwave flux:

$$\frac{1}{\text{OLR}} \frac{d\text{OLR}}{dT_s} + \frac{1}{(1 - \alpha)} \frac{d\alpha}{dT_s} > 0. \quad (1)$$

3. H₂ warming near the inner edge.

3.1. Spectral calculations

It is not obvious that background gases like H₂ or N₂ should have a strong impact near the inner edge of the habitable zone. Earth's greenhouse effect is already dominated by H₂O, and H₂O becomes even more important at higher temperatures. We therefore consider the inner edge for four atmospheric scenarios. First, we consider a pure H₂O atmosphere as the simplest model of the runaway greenhouse (Pierrehumbert 2010; Goldblatt 2015). Second, we consider an Earth-like N₂-H₂O atmosphere with 1 bar of N₂, which is typical of conventional habitable zone calculations (Kast-

ing et al. 1993; Kopparapu et al. 2013). Third, we consider the extreme case of a CO₂-H₂O atmosphere with 1 bar of CO₂. Usually CO₂ concentrations are assumed to be negligibly low near the inner edge of the habitable zone due to the silicate-weathering thermostat (Walker et al. 1981). Here we include CO₂ as a limiting case of a high MMW background gas with a strong greenhouse effect to draw out the distinction between high MMW gases and H₂. Fourth, we consider the new limit of a H₂-H₂O atmosphere with 1 bar of H₂.

Figure 1a shows that in all four scenarios albedo first decreases and then rises again with warming. This behavior is due to the increase of atmospheric water vapor with warming. Below about 250 K all atmospheres contain little water vapor, and are dominated by atmospheric scattering and surface absorption. At these temperatures H₂ creates a significantly higher albedo than both N₂ and CO₂, because H₂ has the highest scattering efficiency among common gases on a per-mass basis (a kg of H₂ contains more molecules than any other gas)³. Above 250 K shortwave absorption increases in the near-IR, where H₂O is a strong absorber, so albedo drops. Above 350 K the atmospheric mass starts to increase in all scenarios, which increases Rayleigh scattering at short wavelengths where H₂O is a relatively poor absorber, so albedo rises again. Finally, above 400 K, all four scenarios become dominated by water vapor so the albedo converges.

Figure 1b shows that OLR in all scenarios approaches a single limiting value at high temperatures. The limiting value at high temperatures is called the runaway greenhouse or Simpson-Nakajima limit (Goldblatt et al. 2013). The runaway arises from the rapid increase of water vapor with warming: once water vapor becomes optically thick at all frequencies, longwave emission decouples from the surface and OLR is determined by the temperature of the upper atmosphere, which is constant once the atmosphere becomes dominated by water vapor (Nakajima et al. 1992; Pierrehumbert 2010; Goldblatt et al. 2013).

The behavior of OLR leading up to the runaway, however, depends strongly on the assumed background gas. The simplest case is a pure H₂O atmosphere, in which OLR approaches the runaway greenhouse monotonically. Adding 1 bar of N₂ does not change OLR much relative to a pure H₂O atmosphere, because N₂ has no strong greenhouse effect of its own, but it introduces an important qualitative difference: N₂ causes OLR to first overshoot the runaway limit before it slowly falls back (Nakajima et al. 1992). Adding 1 bar of CO₂ reduces OLR at low temperatures, due to CO₂'s greenhouse effect, but at high temperatures CO₂ again causes OLR to overshoot the runaway limit. Previous work argued that the overshoot occurs because adding a dry background gas steepens the atmospheric lapse rate relative to that of a steam atmosphere (in the sense of increasing dT/dp ; Nakajima et al. 1992; Pierrehumbert 2010). This means the upper atmosphere is colder for a N₂-H₂O or CO₂-H₂O atmosphere

³ Note that our calculations compare different atmospheric compositions at fixed surface pressure, which is equivalent to holding the total atmospheric mass fixed.

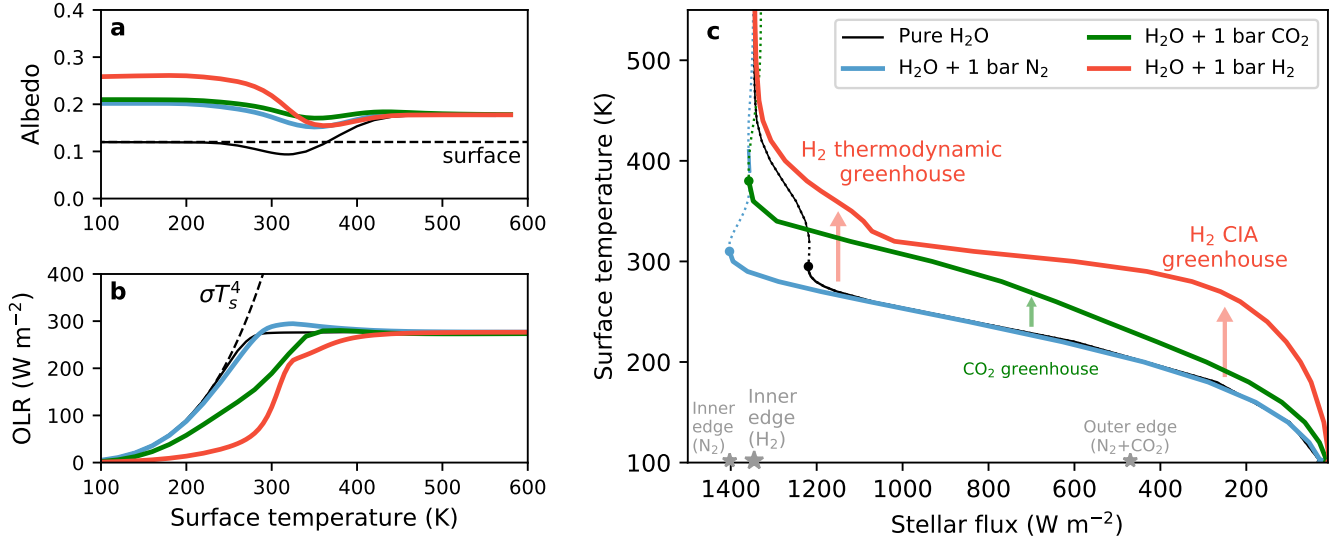


Figure 1. The greenhouse effect of H₂: H₂ causes strong greenhouse warming near the outer edge of the habitable zone due to collision-induced absorption (CIA), but it also causes strong warming near the inner edge of the habitable zone due to its thermodynamic effect. In comparison, CO₂ is a relatively weaker greenhouse gas. (a,b) Albedo and outgoing longwave radiation (OLR) as a function of surface temperature. (c) Surface temperature as a function of received stellar flux. Solid lines are stable, dotted lines are unstable climate states. Grey stars show the conventional inner and outer edge of the habitable zone (Kopparapu et al. 2013), as well as the inner edge for a H₂-rich atmosphere.

than for pure H₂O, which reduces the amount of water vapor in the upper atmosphere and allows the atmosphere to emit more radiation. Importantly, this explanation seems insensitive to the composition of the background gas, so one might expect that H₂ also creates an OLR overshoot.

Surprisingly, we find that OLR changes very differently with warming in a H₂-rich atmosphere (Fig. 1b). At cold temperatures H₂ reduces OLR due to its CIA greenhouse effect. The change in OLR is much larger for 1 bar of H₂ than for 1 bar of CO₂, so on a per-mass basis H₂ is a stronger greenhouse gas than CO₂. Above 250 K OLR shoots up, however, then abruptly flattens out at 320 K, before slowly approaching the runaway limit. Crucially, whereas N₂ and CO₂ cause OLR to overshoot, H₂ causes OLR to undershoot the runaway greenhouse limit. This undershoot strongly affects the climates of H₂-rich atmospheres near the inner edge of the habitable zone.

Figure 1c combines our albedo and OLR calculations, and shows how different background gases influence a planet’s climate stability. We find that N₂-rich and CO₂-rich atmospheres abruptly cease to be stable above surface temperatures of 310 K and 380 K. There are no nearby stable states, so a N₂-rich or CO₂-rich planet transitions from a moderately warm climate straight into the runaway greenhouse and would only re-equilibrate again once the surface temperature exceeds about 1,600 K (Goldblatt et al. 2013). The abrupt onset of the runaway greenhouse in N₂-rich and CO₂-rich atmospheres is largely due to the overshoot in the OLR- T_s curve (Fig. 1b): once peak OLR is reached, the planet cannot emit more longwave radiation with warming, so the only way for the climate to remain stable is by reflecting more sunlight with further warming. Albedo does increase slightly above 350 K, due to increased Rayleigh scattering as the atmosphere thickens, but the albedo increase is small and largely

cancelled by the decrease in OLR with further warming at these high temperatures⁴.

In contrast to high MMW atmospheres, pure H₂O and H₂-rich atmospheres enter the runaway gradually which allows them to sustain unusually warm climates near the inner edge. First, the inner edge of the habitable zone moves slightly outward in pure H₂O and H₂-rich atmospheres when compared to high MMW atmospheres due to the lack of an OLR overshoot. A high MMW background thus allows a planet to remain habitable at moderately higher stellar fluxes than is possible with a pure H₂O or a H₂-rich atmosphere. Focusing on those climates that are inside the habitable zone, however, we find that pure H₂O and H₂-rich atmospheres can sustain much higher surface temperatures than high MMW atmospheres. For example, an atmosphere with 1 bar of N₂ is essentially limited to surface temperatures below 310 K because higher surface temperatures are unstable and lead to further warming. In comparison, an atmosphere with 1 bar of H₂ does not lose its climate stability as it approaches the inner edge, and can sustain surface temperatures of 340 K or more without entering the runaway. This gradual approach to the runaway arises from the OLR undershoot in H₂ (Fig. 1).

To explore how the warming effect of H₂ depends on surface pressure, we performed additional simulations in which we increased the surface pressure of H₂ up to 50 bars. Figure 2 shows that 50 bars of H₂ are sufficient to warm the surface to 450 K or more near the inner edge of the habitable zone. For reference, the critical point of H₂O occurs at about

⁴ Our N₂ calculations do show a small island of stability corresponding to surface temperatures of 390–410 K and stellar fluxes of about 1356–1358 W m⁻². It is highly unlikely that these states would actually be stable: our code still underestimates shortwave absorption in the near UV, and thus produces higher-than-realistic albedos, which would further destabilize warm climates. Moreover, the incident stellar flux would have to be extremely fine-tuned to maintain this state.

647 K. As long as the surface temperature remains below the critical point, a planet can still maintain an ocean and thus remains habitable according to the classical definition of the habitable zone (Kasting et al. 1993). Surface temperatures of 450 K or more, sustained over a timescale of 100 Myrs, would strongly shape a planet’s earliest surface environment and the development of prebiotic chemistry. Moreover, although these temperatures might seem high, the reported upper limit for extant life on Earth is around 400 K (Takai et al. 2008), so these conditions could still be compatible with a thermophile biosphere.

One might think that the strong H_2 warming near the inner edge is caused by H_2 ’s radiative properties. That is not the case. Figure 3 shows that H_2 still leads to strong warming at surface temperatures above 320 K when we disable H_2 - H_2 CIA in our OLR calculations. The inset in Figure 3 shows a measure of the atmosphere’s broadband longwave optical thickness, which we define as $\tau_{LW} = \ln[(\sigma T_s^4)^{-1} \times \int B_\lambda(T_s) e^{-\tau_\lambda} d\lambda]$, where B_λ is the Planck function and τ_λ is the atmospheric optical thickness at a given wavelength λ . The inset shows that the optical thickness of a H_2 -rich atmosphere is due to H_2 ’s CIA opacity below 320 K, but becomes dominated by H_2O opacity at high temperatures. At low temperatures the climate effect of H_2 is therefore due to its role as a greenhouse gas, but at high temperatures its impact must be due to other physics.

3.2. An intuitive explanation for why MMW matters

Why does H_2 lead to strong warming near the inner edge, even without any greenhouse effect of its own, whereas a heavy background gas like N_2 does not? We show next that background gases influence OLR through their influence on an atmosphere’s temperature structure, which we quantify in terms of the thermal scale height. In turn, H_2 ’s ability to inflate the thermal scale height is unique among common atmospheric gases.

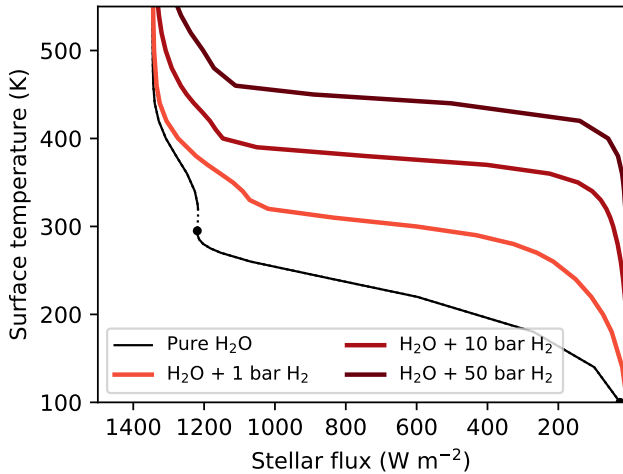


Figure 2. The effect of H_2 at higher surface pressures. 50 bars of H_2 can warm the surface up to 450 K or more. The critical point of H_2O occurs at 647 K. Below the critical point a planet can maintain a liquid surface ocean, and is thus still potentially habitable.

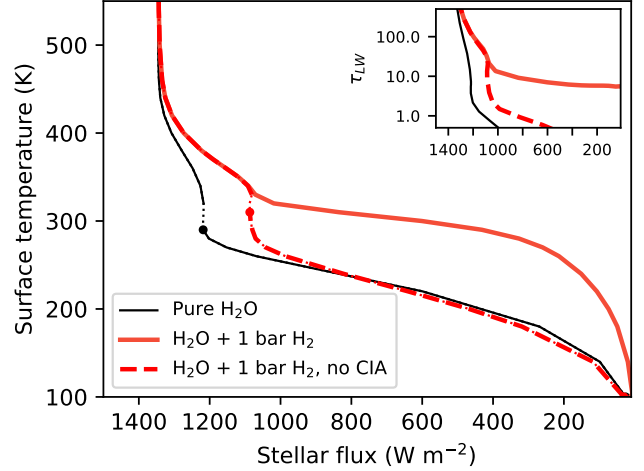


Figure 3. The effect of H_2 near the inner edge is driven by H_2 ’s thermodynamics. The solid red line is our default calculation with H_2 infrared absorption (via H_2 - H_2 collision-induced absorption; CIA), the dashed red line is a test in which we disable H_2 CIA in the longwave. The main plot shows surface temperature, the inset shows optical thickness as a function of stellar flux. Near the inner edge temperature and optical thickness are identical, so H_2 ’s impact near the inner edge is due to its thermodynamic greenhouse instead of its CIA greenhouse effect.

First, the optical thickness of an atmospheric column is directly proportional to the scale height of water vapor. To show this we write the atmosphere’s optical thickness⁵ as

$$\tau = \int_0^\infty \kappa_v \rho_v dz, \quad (2)$$

where z is height, κ_v is the absorption cross-section, and ρ_v is the density of water vapor (in general, the subscript v will denote quantities related to water vapor). We assume κ_v is independent of height and ρ_v decays exponentially following the water vapor scale height H_v , $\rho_v = \rho_{v,0} e^{-z/H_v}$. In general H_v can also vary with height, but due to the exponentially rapid falloff of ρ_v we treat H_v as constant and equal to its value at the surface. We additionally define the absorption length $l_0 \equiv 1/(\kappa_v \rho_{v,0})$, which is the characteristic distance over which a longwave photon is absorbed by the atmosphere. The atmospheric optical thickness is then simply

$$\tau = \kappa_v \rho_{v,0} \int_0^\infty e^{-z/H_v} dz, \quad (3)$$

$$= \frac{H_v}{l_0}. \quad (4)$$

The absorption length l_0 does not depend on background gases, so N_2 or H_2 affect OLR only via changes in the scale height of water vapor H_v .

Next, background gases affect H_v only via changes in the temperature scale height H_T . To show this we start with the general definition for the scale height of water vapor,

$$H_v = \left(\frac{-1}{\rho_v} \frac{d\rho_v}{dz} \right)^{-1}. \quad (5)$$

⁵ Although we will assume grey radiation in the next section, the derivation in this section is general and also holds monochromatically, i.e., at a single wavelength.

We evaluate H_v using the ideal gas law for water vapor, $\rho_v = e^*/(R_v T)$ where e^* is the saturation vapor pressure, and the Clausius-Clapeyron relation, $d \ln e^*/d \ln T = L_v/(R_v T)$ where L_v is the latent heat of vaporization,

$$\frac{1}{\rho_v} \frac{d\rho_v}{dz} = \frac{1}{e^*} \frac{de^*}{dz} - \frac{1}{T} \frac{dT}{dz}, \quad (6)$$

$$= \left(\frac{1}{e^*} \frac{de^*}{dT} - \frac{1}{T} \right) \frac{dT}{dz}, \quad (7)$$

$$= \left(\frac{L_v}{R_v T} - 1 \right) \frac{1}{T} \frac{dT}{dz}, \quad (8)$$

$$\approx \frac{L_v}{R_v T} \frac{1}{T} \frac{dT}{dz}. \quad (9)$$

Here we used $L_v/(R_v T) \gg 1$, which holds for water vapor and a wide range of other condensible gases. We recognize $(-1/T \times dT/dz)^{-1}$ as the temperature scale height H_T , which sets the vertical length scale of temperature decrease, so

$$H_v = \frac{R_v T}{L_v} H_T. \quad (10)$$

Again, R_v , T and L_v are independent of any background gases, so N_2 or H_2 affect optical thickness only via changes in H_T .

Next, we constrain the value of H_T . At cold temperatures water vapor is highly dilute and has essentially no impact on the vertical structure of the atmosphere. In this limit the lapse rate follows the standard dry adiabat, $dT/dz = -g/c_p$, and

$$H_T^{dilute} = \frac{c_p T}{g}. \quad (11)$$

Here c_p is the specific heat capacity of the background gas, e.g., of N_2 .

At high temperatures the atmosphere becomes steam-dominated, and total pressure becomes equal to the saturation vapor pressure of water. In this limit the temperature scale height is equal to

$$H_T^{steam} = -T \frac{dz}{dT}, \quad (12)$$

$$= -T \frac{dz}{de^*} \frac{de^*}{dT}, \quad (13)$$

$$= T \frac{1}{\rho_v g} \frac{L_v e^*}{R_v T^2}, \quad (14)$$

$$= \frac{L_v}{g}, \quad (15)$$

where we used the hydrostatic relation in the third step.

If we evaluate H_T for H_2 versus N_2 , we find that different background gases lead to dramatically different temperature scale heights. With an Earth-like gravity and at a temperature of 300 K, $H_T^{dilute} \approx 30$ km in N_2 , whereas $H_T^{dilute} \approx 430$ km in H_2 . The difference arises from the low molecular

weight of H_2 relative to that of N_2 . Even though both are diatomic molecules with similar degrees of freedom, one kilogram of H_2 contains 14 times more molecules than one kilogram of N_2 , which means the specific heat capacity c_p of H_2 is roughly 14 times larger than that of N_2 .

Now, as both N_2 and H_2 atmospheres warm up, they eventually end up being dominated by water vapor. The temperature scale height of a steam atmosphere is $H_T^{steam} \approx 250$ km. This means H_T grows with warming if an atmosphere starts out N_2 -rich, but H_T shrinks with warming if the atmosphere starts out H_2 -rich.

Because H_T controls H_v , and therefore the atmosphere's optical thickness τ , we see that warming leads to a compositional climate feedback which depends on the molecular weight of the background gas. An N_2 -rich atmosphere starts out dense and compact, with a small thermal scale height H_T . Warming moves the atmospheric composition closer to the steam limit, so H_T increases. This implies H_v also increases with warming, so moving from a N_2 -rich to a H_2O -rich atmosphere means the atmosphere moistens even faster than a pure H_2O atmosphere would. The moistening increases τ , tends to reduce OLR, and thus acts to amplify warming.

In contrast, a H_2 -rich atmosphere starts out with a large scale height H_T . Warming moves the atmospheric composition closer to the steam limit, so H_T and H_v eventually have to decrease. Consequently, the shift from H_2 to H_2O means the atmosphere moistens less quickly than a pure H_2O or a N_2 -rich atmosphere does – a stabilizing climate feedback.

The existence of this feedback, and its sensitivity to the MMW of the background gas, provide a first clue as to why H_2 -rich atmospheres become much warmer than N_2 -rich, or even CO_2 -rich, atmospheres (Fig. 1). Moreover, the sign of this feedback appears to be stabilizing only for H_2 . Even if we consider Helium as the next-heavier background gas after H_2 , such as a remnant atmosphere clinging to the core of an evaporated mini-Neptune (Hu et al. 2015), we find $H_T^{dilute} \approx 160$ km, which is smaller than $H_T^{steam} \approx 250$ km. The compositional feedback therefore requires the molecular weight of the background gas to be small enough so that the sensible heat of the background gas, $c_p T$, becomes larger than the latent heat of steam, L_v . H_2 appears to be unique in this regard, which means H_2 -rich habitable atmospheres are distinct in terms of generating a stabilizing feedback as they transition from a cold, dry climate to a hot, steam-dominated climate.

4. New climate states in H_2 -rich atmospheres

Different background gases have a strong influence on a planet's climate, so can we understand their effect more generally? In this section we first present grey radiative calculations which qualitatively recover the onset of the runaway greenhouse in our spectral calculations, and which therefore allow us to understand in detail how different background gases affect the inner edge of the habitable zone (Section 4.1). Second, we present analytical results which explain why OLR overshoots the runaway limit with a high MMW gas like N_2 , but undershoots the runaway limit with H_2 . In

doing so we present a new climate state which we call the dilute runaway, and elucidate its underlying physics (Sections 4.2 and 4.4). Third, we discuss how H_2 's thermodynamics give rise to a non-monotonic climate feedback which we call the Soufflé effect (Section 4.3). Finally, the calculations in this section assume idealized grey radiation, which allows us to understand the thermodynamic effect of different background gases, but do not capture all aspects of our spectral calculations. We discuss the remaining differences between grey and spectral calculations at the end of this section (Section 4.5).

4.1. Numerical calculations

For our grey radiative calculations we use the same grey longwave opacity for water vapor as in Nakajima et al. (1992), $\kappa_v = 0.01 \text{ m}^2 \text{ kg}^{-1}$. The background gas is assumed to be completely transparent to longwave radiation, so its only influence on OLR is via its influence on the atmosphere's temperature structure. The colored lines in Figure 4 show the response of OLR to warming for three different atmospheric compositions: a pure H_2O atmosphere, a N_2 -rich atmosphere, and a H_2 -rich atmosphere. We vary the surface pressure of the background gas between 0.1 and 10 bar for H_2 and 0.1 and 100 bar for N_2 .

Figure 4 recovers the main qualitative features of our spectral calculations. First, the OLR of a grey pure H_2O atmosphere closely resembles our spectral calculations for pure H_2O (Fig. 1). At temperatures below about 250 K there is little water vapor in the atmosphere, the atmosphere is largely transparent to longwave radiation, and most emission originates from the surface, so $\text{OLR} \approx \sigma T_s^4$. With further warming the atmosphere rapidly becomes optically thick and monotonically approaches a limiting value of about 290 W m^{-2} . This limiting OLR has previously been called the Simpson-Nakajima limit (Goldblatt et al. 2013), for reasons we explain below we will call it here the “steam limit”. Second, adding N_2 as a background gas leads to an overshoot and allows OLR to exceed the steam limit, as in our spectral calculations. Adding H_2 has a similar but opposite effect, in which OLR undershoots the steam limit.

Figure 4 also shows several new features which we did not find in our spectral calculations. Although some of these features are sensitive to the details of our radiative assumptions (see Section 4.5), we focus on them here because they allow for important insight into the thermodynamic effect of different background gases. In particular, at moderate surface temperatures and high surface pressures, OLR hits an asymptotic limit that is distinct from the steam limit. This new OLR limit is higher than the steam limit for N_2 and lower for H_2 . The temperature range over which OLR remains close to this limit depends on the amount of background gas. For example, atmospheres with less than 1 bar of background gas do not reach this limit whereas an atmosphere with 100 bar of N_2 remains at this limit for more than 100 K. We note that this asymptotic limit is distinct from the Komabayashi-Ingersoll limit (Komabayashi 1967; Ingersoll 1969), which re-

quires a stratosphere, whereas our calculations do not include a stratosphere (we discuss this point in Section 5).

The asymptotic OLR limit at high surface pressures was first discussed by Nakajima et al. (1992). Imagine a moderately warm planet with large amounts of dry background gas, so that its atmosphere contains some H_2O but water vapor does not yet affect the temperature structure and the lapse rate is still dry-adiabatic. As the planet warms beyond a threshold (e.g., $\sim 300 \text{ K}$ in our spectral calculations; Fig. 1), water vapor becomes optically thick and the planet's OLR decouples from the surface temperature. In this case the atmosphere's emission temperature remains constant with warming – the planet is in a runaway state. The invariance to warming is only disrupted once water vapor reaches a sufficient abundance to affect the lapse rate, and thus modify the temperature at the emission level. Because this radiation limit resembles the runaway greenhouse, but requires enough background gas so that H_2O is dilute compared to the background gas, we call this OLR limit the “dilute runaway”. The dilute runaway stands in contrast to the traditional Simpson-Nakajima runaway in which the atmosphere is dominated by water vapor, and which we call the “steam runaway”.

Nakajima et al. (1992) discussed the physics that can lead to the dilute runaway, but did not discuss its physical relevance in detail. Below we show that the dilute runaway, and how it depends on atmospheric MMW, is the underlying reason why H_2 -rich atmospheres approach the steam runaway gradually, whereas N_2 -rich atmospheres are unstable at high temperatures and enter the steam runaway abruptly.

4.2. The dilute runaway

As an atmosphere warms its OLR first tends towards the dilute limit, and then towards the steam limit (Fig. 4). If one could derive a simple expression for OLR in both limits, one could therefore predict whether a background gas causes an atmosphere to over- or undershoot the steam limit. In this section we do so, by deriving a closed-form analytical expression for the OLR of a runaway greenhouse atmosphere which was previously only solved implicitly (Nakajima et al. 1992; Pierrehumbert 2010).

First, we derive an approximate form of the Clausius-Clapeyron relation. The Clausius-Clapeyron relation is often written as $d \ln e^* / d \ln T = L_v / (R_v T)$, which can be integrated to solve for $e^*(T)$. This form of $e^*(T)$ does not lead to closed-form expressions for optical thickness and OLR, however, so we instead treat the right-hand side as constant, $d \ln e^* / d \ln T \approx L_v / (R_v T_0) \equiv \gamma$. In this case e^* becomes a simple power law,

$$e^* = e_0^* \left(\frac{T}{T_0} \right)^\gamma. \quad (16)$$

Here γ controls how rapidly saturation vapor pressure increases with temperature, and T_0 is a reference temperature which we will pick to be close to the temperature range of interest.

Our approximation allows us to express the relation between optical thickness and temperature as a power law,

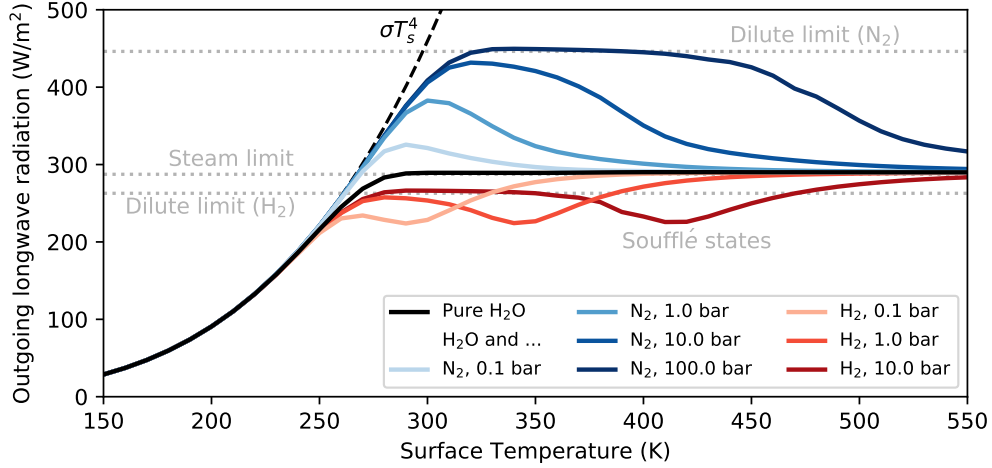


Figure 4. Background gases can have a strong influence on a planet’s outgoing longwave radiation (OLR). Colors show grey calculations with N_2 and H_2 backgrounds, grey shows analytical results which we derive in Section 4.2. OLR tends towards the steam limit at high temperatures, but at moderate temperatures and high surface pressures we find an additional “dilute runaway” limit. The dilute limit in N_2 is greater than the steam limit, so N_2 atmospheres overshoot the steam limit, whereas in H_2 it is less than the steam limit, so H_2 atmospheres undershoot. In addition, the transition from the dilute limit to the steam limit in H_2 is non-monotonic due to the “Soufflé effect” (Sec. 4.3).

which turns out to be highly useful. We combine Equation 4 with the ideal gas law for water vapor, $\rho_v = e^*/(R_v T)$. We find

$$\tau = \kappa_v H_v \rho_v, \quad (17)$$

$$= \kappa_v H_T \frac{e^*}{L_v}, \quad (18)$$

$$= \kappa_v H_T \frac{e_0^*}{L_v} \times \left(\frac{T}{T_0}\right)^\gamma. \quad (19)$$

This expression depends on atmospheric composition and background gases only through the temperature scale height H_T . As we showed before, $H_T^{dilute} = c_p T/g$ and $H_T^{steam} = L_v/g$. If we further approximate the temperature dependency of H_T^{dilute} as $H_T^{dilute} \approx c_p T_0/g$, we can express τ as single power law in both limits,

$$\tau = \tau_0 \left(\frac{T}{T_0}\right)^\gamma. \quad (20)$$

Here $\tau_0 = (c_p T_0/L_v) \times \kappa_v e_0^*/g$ in the dilute limit while $\tau_0 = \kappa_v e_0^*/g$ in the steam limit.

We are now able to find a closed solution for the runaway greenhouse radiation limit. For a grey gas, OLR is equal to

$$\text{OLR} = \sigma T_s^4 e^{-\tau} + \int_0^\tau \sigma T(\tau')^4 e^{-\tau'} d\tau'. \quad (21)$$

As the atmosphere becomes optically thick the surface contribution from the first term can be neglected and the inte-

gral’s upper limit replaced with infinity,

$$\text{OLR}_\infty \approx \int_0^\infty \sigma T(\tau)^4 e^{-\tau} d\tau, \quad (22)$$

$$= \sigma T_0^4 \int_0^\infty \left(\frac{\tau}{\tau_0}\right)^{4/\gamma} e^{-\tau} d\tau, \quad (23)$$

$$= \sigma T_0^4 \tau_0^{-4/\gamma} \int_0^\infty \tau^{4/\gamma} e^{-\tau} d\tau, \quad (24)$$

$$\text{OLR}_\infty = \sigma T_0^4 \times \frac{\Gamma(1 + 4/\gamma)}{\tau_0^{4/\gamma}}. \quad (25)$$

Here Γ is the gamma function, and τ_0 is defined as

$$\tau_0 = \begin{cases} \frac{\kappa_v e^*(T_0)}{g}, & \text{steam limit} \\ \frac{\kappa_v e^*(T_0) c_p T_0}{g L_v}, & \text{dilute limit.} \end{cases} \quad (26)$$

Our solution in Equation 25 has a similar form to Pierrehumbert (2010)’s solution for the OLR of a dry atmosphere, but instead holds for a moist runaway atmosphere.

To evaluate our solution we only need to choose a reference temperature T_0 where our approximation of Clausius-Clapeyron will be most accurate. For the runaway greenhouse T_0 should be close to the surface temperature at which the atmosphere becomes optically thick. A convenient choice for all three atmospheric scenarios is the temperature at which the optical thickness of a pure- H_2O atmosphere equals unity.

Figure 4 compares our analytical solution against our numerical calculations. We find that the analytical solution closely match the numerical results, so our expression successfully captures the physics of both the dilute and the steam runaway.

Our solution now allows us to understand why OLR overshoots in a N_2 -rich atmosphere but undershoots in a H_2 -rich atmosphere (Fig. 4). The reference temperature T_0 is

independent of the background gas, so the greater value of OLR_∞ for N_2 relative to H_2 depends entirely on τ_0 . In turn, background gases only affect τ through the temperature scale height H_T . The ratio of optical thicknesses in the dilute versus the steam limit is

$$\frac{\tau_{\text{dilute}}}{\tau_{\text{steam}}} = \frac{H_T^{\text{dilute}}}{H_T^{\text{steam}}}, \quad (27)$$

$$= \frac{c_p T_0}{L_v}, \quad (28)$$

which expresses our result from Section 3.2 in terms of a single non-dimensional parameter. Again, for H_2O condensing in N_2 at around 300 K this ratio is less than unity, $c_p T_0/L_v \sim 0.1$, whereas in H_2 this ratio is $c_p T_0/L_v \sim 1.7$. Comparing the two values, the ratio is closer to unity for H_2 than for N_2 , which explains why the OLR undershoot in H_2 is small whereas the OLR overshoot in N_2 is large (Fig. 4). Moreover, as we showed in Section 3.2, H_2 's impact as a background gas is essentially unique. Even if we consider condensable gases other than H_2O , we are not able to find a likely combination for which $c_p T_0/L_v > 1$ without H_2 as the background gas⁶. Conversely, even if we consider gases other than H_2O that could condense in a H_2 -rich atmosphere (e.g., an early Titan with a H_2 atmosphere and a CH_4 surface ocean, or a super-Mars with a H_2 atmosphere and large CO_2 glaciers), we find that $c_p T_0/L_v > 1$ for all these condensable substances.

In conclusion, H_2 is the only common background gas for which the dilute runaway limit lies below the steam limit, which explains why H_2 -rich atmospheres approach the runaway greenhouse gradually while all high MMW atmospheres enter the runaway greenhouse abruptly. Next, we show why the evolution of OLR is not monotonic with warming in a H_2 atmosphere.

4.3. Non-monotonic OLR: the Soufflé Effect in H_2

In the previous section we derived asymptotic expressions for the dilute and steam limits. In this section we go one step further and consider first-order effects that appear when an atmosphere is slightly warmer than the cold dilute limit, or slightly colder than the hot steam limit. We find two thermodynamic feedbacks that shape the evolution of OLR with warming, and that explain the non-monotonicity of OLR in H_2 (Fig. 4).

At relatively low temperatures, we find that the latent heat release of water vapor dominates over water vapor's other thermodynamic effects. This means the addition of water vapor will always first warm and moisten an atmosphere, regardless of the dry background gas. As proof we consider the general moist adiabat (Pierrehumbert 2010; Ding & Pierrehumbert 2016) in the limit of a nearly dry atmosphere. We perform a series expansion, assuming the molar mixing ratio

is small, $e^*/p_d \ll 1$, and additionally use $L_v/(R_v T) \gg 1$ (which holds for a wide range of condensibles) while R/c_p is always of order unity. We find

$$\left. \frac{dT}{dp} \right|_{\text{dilute}} \approx \frac{R_d T}{c_p p} \times \left(1 - \frac{R_d}{c_p} \left(\frac{L_v}{R_v T} \right)^2 \frac{e^*}{p} \right). \quad (29)$$

By combining this result with the hydrostatic relation for dry air we can solve for the thermal scale height in the near-dilute limit,

$$H_T = -T \frac{dz}{dp} \frac{dp}{dT}, \quad (30)$$

$$= \frac{c_p T}{g} \left(1 + \frac{R}{c_p} \left(\frac{L_v}{R_v T} \right)^2 \frac{e^*}{p} \right). \quad (31)$$

Here the factor $R_d/c_p \times (L/(R_v T))^2 \times e^*/p$ captures the first-order thermodynamic effect of water vapor. Because $R_d/c_p \times (L/(R_v T))^2 \times e^*/p$ is always positive, it acts to increase H_T and thus τ . Intuitively, adding trace amounts of water vapor to a dry parcel releases latent heat, which decreases the lapse rate and allows the atmospheric column to hold more water vapor. This provides a moistening feedback which increases H_v and τ , and thus decreases OLR. Importantly, the moistening feedback is largely independent of background gas because the background gas only appears via the parameter R_d/c_p which is approximately constant (e.g., $R_d/c_p = 2/5$ for He, whereas $R_d/c_p \approx 2/7$ for N_2 or H_2). This feedback explains why, after an atmosphere hits the dilute runaway, further warming then leads to a OLR decrease in both N_2 - and H_2 -rich atmospheres (Figure 4).

At high temperatures the compositional feedback we already described in Section 3.2 dominates. To quantify it we consider the effect of a background gas on the mean molecular weight of a steam atmosphere, which shows up via the gas constant used in the hydrostatic relation, and perform a series expansion in the limit $p_d/e^* \ll 1$. We find

$$\left. \frac{dp}{dz} \right|_{\text{steam}} = -\bar{\rho}g, \quad (32)$$

$$\approx \rho_v g \times \left(1 + \frac{R_d - R_v p_d}{R_d e^*} \right) \quad (33)$$

We solve for the thermal scale height by combining this result with the lapse rate of a steam atmosphere and find

$$H_T = \frac{L_v}{g} \left(1 + \frac{R_d - R_v p_d}{R_d e^*} \right). \quad (34)$$

The sign of $(R_d - R_v)/R_d \times p_d/e^*$ depends on the MMW of the background gas, so a background gas can either increase or decrease H_T and τ near the steam limit. For N_2 in H_2O , $R_d < R_v$, so N_2 has a net drying effect. However, as a steam atmosphere warms, this drying effect weakens and τ will increase even faster than it would in a pure H_2O atmosphere - a positive feedback, just as in Section 3.2. In contrast, H_2 has a net moistening effect because $R_v < R_d$. This

⁶ For CO_2 condensing in a CH_4 -rich atmosphere, $c_p T_0/L_v \sim 1.1$ due to CO_2 's small latent heat combined with CH_4 's relatively small MMW. However, such an atmosphere would likely not be chemically stable unless it was constantly replenished through a disequilibrium process.

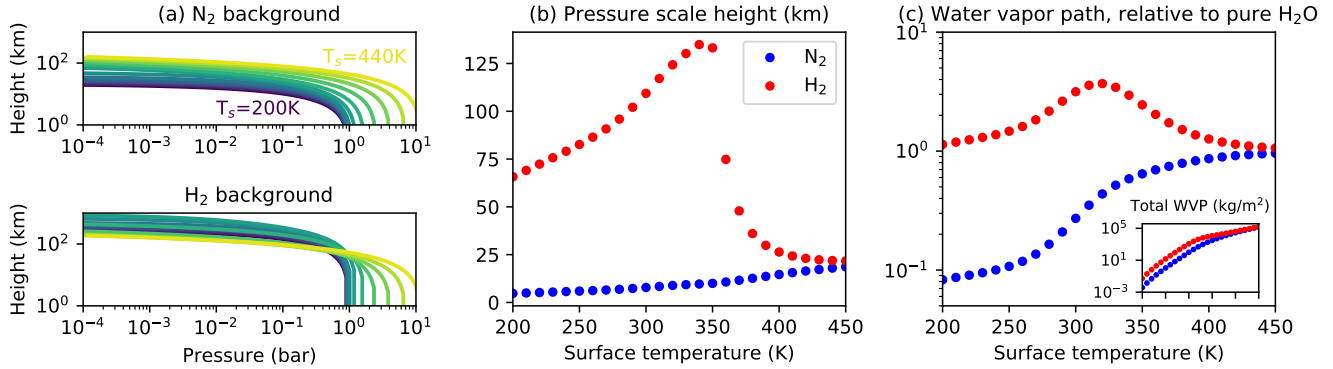


Figure 5. The Soufflé effect: in a H₂-rich atmosphere, moderate warming increases the atmospheric water vapor, which releases latent heat and puffs the atmosphere up further. However, strong warming collapses the atmosphere, once heavy water vapor and condensation start to dominate over light H₂ and dry convection. In contrast, N₂-rich atmospheres puff up monotonically. a) Pressure-height profiles as a function of surface temperature. b) Average pressure scale height, $p_s^{-1} \int (-1/p \times dp/dz)^{-1} dp$, versus surface temperature. c) The atmospheric water vapor path (WVP) as function of surface temperature, relative to the WVP of a pure H₂O atmosphere. Inset shows absolute values of WVP.

effect weakens with warming, which slows the increase of τ relative to that in a pure H₂O atmosphere, and thus provides a negative feedback.

For a N₂-dominated atmosphere, both the latent heating feedback in Equation 31 and the drying feedback in Equation 34 have the same sign with warming and act to decrease OLR. That is why, after an initial overshoot, OLR decreases monotonically towards the steam limit (Figure 4). Conversely, for a H₂-dominated atmosphere the latent heating feedback first decreases OLR before the moistening feedback eventually sets in and causes OLR to rise again.

Based on what a H₂-rich atmosphere looks like as it warms up, we call its temperature-dependent succession of feedbacks the ‘‘Soufflé effect’’. Figure 5 shows how the Soufflé effect plays out in our calculations. As the atmosphere warms up, the pressure scale height increases. At cold temperatures this increase is linear with temperature, and arises from the atmosphere’s thermal expansion. Starting at 280 K the H₂-rich atmosphere begins to puff up a lot faster. This effect is due to the latent heat release of water vapor, which moistens the atmosphere and reduces OLR (Fig. 4). However, just as too much steam causes a Soufflé to collapse, too much steam becomes fatal for a H₂-rich atmosphere: once heavy condensing H₂O begins to displace light dry H₂, at around 340 K, the atmospheric scale height collapses. This collapse slows down the further increase of atmospheric water and increases OLR (compare Fig. 4 and Fig. 5b).

4.4. How much dry background gas is required?

We have shown that different background gases can have a major influence on a planet’s climate, but how much background gas is required for this influence to become apparent? We address this question by considering whether an atmosphere can transition straight from a cold climate into the steam runaway, or whether it enters a dilute runaway phase first.

To enter either runaway state the atmosphere first needs to become optically thick so that OLR decouples from the

planet’s surface emission, which means

$$\tau_{LW}(T_1) > 1. \quad (35)$$

Here T_1 is the surface temperature necessary so that the overlying atmospheric column contains enough water vapor to be optically thick. For example, with a grey absorption cross-section of $\kappa_v = 0.01 \text{ m}^2 \text{ kg}^{-1}$, $T_1 \sim 310 \text{ K}$ in a thick N₂ background and $T_1 \sim 270 \text{ K}$ in a thick H₂ background. In general T_1 depends on the detailed radiative properties of the condensing gas. However, it turns out that several condensible greenhouse gases start to become optically thick roughly around surface temperatures corresponding to their triple point (see SI in Koll & Cronin 2018). In the following we therefore approximate T_1 as the triple point temperature of each condensible gas⁷.

To sustain the dilute runaway an atmosphere needs to have sufficient background gas, otherwise it only experiences a transient overshoot/undershoot (Fig. 4). We quantify the required amount of background gas by considering the first-order correction term to the dry adiabat in Equation 29, which is equal to $R_d/c_p \times (L_v/(R_v T))^2 \times e^*/p$. For the atmosphere to be dilute this term has to be much less than unity, which

| Condensing gas | Dilute Runaway | Steam Runaway |
|------------------|--------------------------------|-----------------------------|
| | $p_{s,dry}$ greater than (bar) | $p_{s,dry}$ less than (bar) |
| H ₂ O | 2.0 | 0.004 |
| CH ₄ | 13 | 0.05 |
| NH ₃ | 16 | 0.03 |
| CO ₂ | 420 | 4.8 |

Table 1. An atmosphere’s dry background pressure determines whether an atmosphere can enter a dilute runaway, or transitions directly into the steam runaway. For the dilute runaway we assume a diatomic background gas, $R_d/c_p=2/7$, for the steam runaway we use N₂ as the background gas.

⁷ By equating T_1 with the triple point, our criterion is overly stringent for H₂O: H₂O’s triple point is 273 K, whereas the H₂O runaway occurs at around 310 K in a saturated N₂-rich atmosphere (Koll & Cronin 2018).

leads to the following threshold on the dry (background) surface pressure,

$$p_{s,dry} \gg \frac{R_d}{c_p} \left(\frac{L_v}{R_v T_1} \right)^2 e^*(T_1). \quad (36)$$

Conversely, if the background pressure is very low the atmosphere transitions from a cold climate straight into the steam runaway. Equation 33 shows that the first-order correction term near the steam limit is equal to $(R_d - R_v)/R_d \times p_d/e^*$, which leads to the following threshold,

$$p_{s,dry} \ll \frac{R_d}{R_d - R_v} e^*(T_1). \quad (37)$$

We evaluate the thresholds from Equations 36 and 37 in Table 1, replacing inequalities with a factor of three.

Table 1 shows that even small amounts of dry background gas are sufficient to modify the behavior of a steam atmosphere, while moderately large amounts of dry background gas can sustain a dilute runaway. A few millibar of dry background gas, or about the surface pressure of Mars, already suffice to modify the H₂O steam runaway. This value increases to several bar of dry gas for CO₂, while methane and ammonia are intermediate between the two. It is thus relatively easy for a minor background gas to modify the OLR of a condensible-rich atmosphere. Of course, the exact climatic impact of the background gas (i.e., whether it creates an OLR overshoot or undershoot) depends on its MMW. The dilute runaway is easiest to achieve for H₂O, with around two bar of dry background gas, and most difficult to achieve for CO₂, with several hundred bar of dry background gas (Table 1). The difference between condensible gases is primarily driven by the triple point vapor pressures, with a small vapor pressure for H₂O and a large vapor pressure for CO₂.

To put these calculations into context, present-day Earth has 1 bar of N₂-O₂ background while Titan has about 1.5 bar of N₂. In both cases there is enough dry background gas to significantly affect the atmosphere’s thermal structure and OLR, but both fall short of the dilute runaway threshold for H₂O and CH₄. In contrast, Venus’ atmosphere currently has about 3 bar of N₂ background pressure. If this N₂ entered the atmosphere early in the planet’s history, it could have had a significant influence on the onset of the runaway greenhouse on Venus.

4.5. Explaining the difference between grey and spectral calculations

The comparison between Figures 1 and 4 shows that H₂ atmospheres undershoot the steam limit as our grey model predicts. However, unlike our grey calculations, our spectrally-resolved calculations do not enter a dilute runaway and, for H₂-rich atmospheres, do not show a non-monotonic OLR with warming.

The difference between our grey and our spectral calculations arises from the opacity of the background gas. Whereas our grey calculations assume that any background H₂ is transparent in the infrared, H₂ actually has a strong CIA

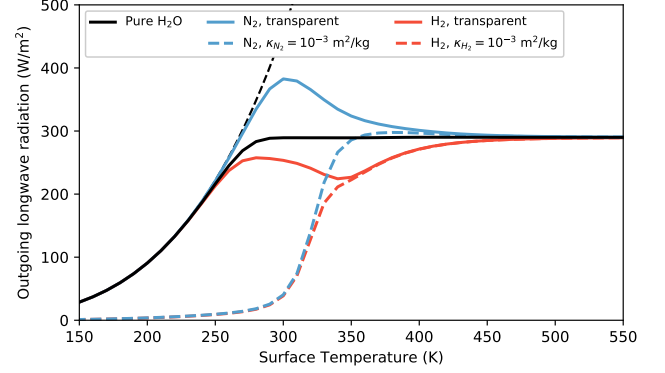


Figure 6. The dilute runaway is no longer accessible if the background is also a strong grey infrared absorber. Solid lines assume that H₂O is the only absorbing gas (H₂ or N₂ are transparent), dashed lines assume that there is additional absorption from the background gas.

greenhouse effect which is dominant at cold surface temperatures. In a H₂-rich atmosphere the impact of H₂O is thus first felt via the impact of H₂O condensation on the lapse rate (Section 4.3), which influences the temperature of the emission level. It is only at relatively high surface temperatures that H₂O starts to be the dominant opacity source at the emission level so that OLR approaches the steam runaway.

To illustrate how H₂’s greenhouse effect affects our grey calculations, we repeat them with a dry background gas that is opaque in the longwave. This is a general proxy for cases in which the atmosphere’s background greenhouse effect is non-zero but remains fixed with surface temperature (e.g., atmospheres dominated by H₂ or CO₂, but also Earth-like atmospheres with a mixed N₂-CO₂ background). We use the following opacities, $\kappa_v = 10^{-2} \text{ m}^2 \text{ kg}^{-1}$ and $\kappa_{dry} = 10^{-3} \text{ m}^2 \text{ kg}^{-1}$. With 1 bar of dry background gas, this means the atmosphere has an optical thickness of about 10 even without any water vapor.

Figure 6 shows why a background greenhouse gas is sufficient to obscure the dilute runaway and any non-monotonic OLR evolution with warming. At cold temperatures the atmosphere is already optically thick, and OLR is substantially lower than the surface emission σT_s^4 . Instead of entering the dilute runaway at around 270 K, OLR stays low until shooting up at around 300 K. The rapid increase occurs because the reduction of the lapse rate with surface warming (see Section 4.3) causes the atmosphere’s emission temperature to increase faster than the surface temperature. With sufficient warming H₂O dominates the opacity near the emission level, at which point calculations with an opaque background become identical to calculations with a transparent background (Fig. 6). Further warming then results in the familiar asymptote of OLR towards the steam limit.

Figure 6 also shows how additional greenhouse gases affect the initiation of the runaway greenhouse in a high MMW atmosphere, such as adding CO₂ to a N₂-rich atmosphere. With a transparent N₂-rich background the OLR overshoot is large and the OLR “bump” occurs at a low temperature of about 300 K, whereas with an optically thick N₂-rich background the amplitude of the overshoot shrinks and the OLR

bump moves to about 370 K. Additional greenhouse gases such as CO_2 can therefore shift the initiation of the runaway to higher temperatures in a N_2 -rich atmosphere, but they do not alter our result that high MMW atmospheres experience an OLR overshoot whereas H_2 -rich atmospheres experience an OLR undershoot.

In conclusion, H_2 's CIA greenhouse explains why the dilute runaway is not directly apparent in our spectral calculations for H_2 -rich atmospheres. Nevertheless, the dilute runaway is still a useful theoretical limit because it provides a simple way of understanding why different background gases lead to an OLR overshoot or undershoot, and thus explains why N_2 -rich atmospheres abruptly jump from temperate climates into the steam runaway, whereas H_2 -rich atmospheres approach the steam runaway smoothly (Figure 1). Similarly, although H_2 's CIA greenhouse prevents OLR from becoming non-monotonic, the stabilizing climate feedback induced by the Soufflé effect is the underlying reason why H_2 atmospheres can remain stable at extremely elevated surface temperatures. Finally, Soufflé dynamics also shape the remote appearance of H_2 atmospheres, which would be important for interpreting potential transit observations of H_2 -rich exoplanets.

5. Discussion

We have shown that H_2 leads to a number of novel thermodynamic feedbacks that allow terrestrial planets with H_2 -rich atmospheres near the inner edge of the habitable zone to sustain hot surface climates. Our work relates to previous studies on the origin of life and the habitability of H_2 climates in multiple ways:

Previous work on the origin of life. Our work has interesting consequences for early Earth. Several bars of H_2 are sufficient to create global-mean surface temperatures above 60°C , either via a direct H_2 - H_2 greenhouse or through H_2 's amplification of the H_2O greenhouse (Fig. 1). Such a hot start for life is compatible with the view that the last common ancestor of life on Earth was a thermophile (Giulio 2003), and has the additional benefit that hot surface conditions could have dramatically accelerated prebiotic chemical reactions (Stockbridge et al. 2010). By the same token life would also experience a hot start on habitable evaporated cores, i.e., mini-Neptunes which lost their hydrogen envelopes and turned into super-Earths (Luger et al. 2015). Theoretical predictions and exoplanet observations suggest that this formation pathway is common (Lopez et al. 2012; Fulton & Petigura 2018), so many habitable-zone planets would have sustained thick hydrogen envelopes early on. As a mini-Neptune loses its hydrogen and surface conditions drop below the critical point of H_2O (~ 220 bar, 647 K), the planet would be able to sustain a liquid ocean. As long as any remnant H_2 persists, however, the planet's surface would remain hot (Fig. 1). Life on H_2 -rich exoplanets would thus arise under hyperthermal and reduced conditions, but might subsequently struggle to adapt to the planet's gradual cooling and oxidation as the atmospheric hydrogen was lost to space (see Wordsworth 2012; Abbot 2015).

Previous work on H_2 climates. Our results complement previous work on the impact of H_2 in colder climates, where its strong CIA greenhouse effect is dominant. Several previous studies considered H_2 -rich atmospheres but assumed a fixed dry adiabatic temperature structure in their calculations (Pierrehumbert & Gaidos 2011; Wordsworth 2012), which precluded them from identifying the unusual climate feedbacks and Soufflé dynamics of H_2 atmospheres we discuss here. Other studies included full moist thermodynamics but limited themselves to atmospheres in which H_2 did not dominate the mass of the assumed background gas (Wordsworth & Pierrehumbert 2013; Ramirez et al. 2014; Batalha et al. 2015; Ramirez & Kaltenecker 2017), so these studies could similarly not identify the feedbacks that occur once H_2 becomes the dominant background gas.

Finally, our results could be affected by additional physics as follows:

Lifetime of H_2 atmospheres. Our observation that young H_2 -rich atmospheres can be sustained long enough to influence the origin of life is sensitive to a number of factors. One important factor is the planet's host star. We considered planets around Sun-like stars, but planets around M dwarfs would lose hydrogen much more rapidly due to the elevated XUV emission of young M dwarfs (Penz et al. 2008). Nevertheless, even in this case some rocky planets around M dwarfs might outgas sufficient hydrogen during the solidification of the magma ocean to set the stage for an early H_2 -rich climate (Elkins-Tanton & Seager 2008). Another important factor is the formation time of the planet's hydrogen envelope. Since H_2 is constantly escaping to space, and since the host star's XUV flux diminishes rapidly over time, any delay in outgassing would substantially lengthen the lifetime of a H_2 atmosphere. For example, this might be possible if hydrogen was produced by a very late giant impact, several hundred million years after the star's formation (e.g., Quintana et al. 2016).

Mixed backgrounds. Although we have focused on pure background compositions, it is straightforward to extend our results to atmospheres with mixed compositions such as a primordial H_2 -He or a H_2 - N_2 atmosphere. Equation 28 shows that in this case the mass-weighted mean heat capacity, \bar{c}_p , compared to the ratio L_v/T determines whether the background gas leads to an OLR overshoot or undershoot. Evaluating this criterion for a wide range of mixed backgrounds, we find that the OLR undershoot remains robust as long as H_2 dominates the background's overall mass (i.e., as long as H_2 's mass mixing ratio exceeds 50-55%). In the scenario of early Earth with 1 bar of N_2 , the addition of slightly more than 1 bar of H_2 would thus be sufficient to create an atmosphere with climate feedbacks that are driven by H_2 thermodynamics.

Stratospheres. Our calculations assume an all-adiabat atmosphere and neglect the radiative impact of a stratosphere. To test our results we repeated our grey radiative calculations with a stratosphere. We find that our results are largely robust, even though the addition of a stratosphere lowers OLR in the dilute runaway limit while barely affecting OLR in

the steam runaway limit. The underlying reasons for how a stratosphere affects our grey calculations are not easily summarized, and will be explained in a forthcoming paper (Koll & Cronin, in prep). Here we simply note that there is an intimate connection between our results for the dilute runaway and previous work on the Komabayashi-Ingersoll (KI) limit, which is a runaway limit analogous to the steam runaway but which considers only the stratosphere's radiative balance (Komabayasi 1967; Ingersoll 1969).

Additional effects of H₂. More work is needed to explore additional effects which we were not able to address in this study. Previous work on the runaway greenhouse in N₂-rich atmospheres underlined that sub-saturation and clouds can have a large impact on the runaway greenhouse threshold (Pierrehumbert 1995; Leconte et al. 2013; Yang et al. 2013). Similarly, moist convection could develop strong spatial and time variability in H₂-dominated atmospheres (Li & Ingersoll 2015). These dynamics cannot be fully represented in 1D equilibrium models. Our study is therefore only a first look at hot habitable climates in hydrogen-dominated atmospheres, and should be followed up with 3D modeling.

We thank Edwin Kite and Sara Seager for detailed feedback and helpful discussions, and an anonymous reviewer for valuable comments. This article uses the ApJ template⁸. D.D.B.K. was supported by a James S. McDonnell Foundation postdoctoral fellowship. T.W.C. was supported by NSF grant AGS-1623218.

References

- Abbot, D. S. 2015, *The Astrophysical Journal Letters*, 815, L3
- Barber, R. J., Tennyson, J., Harris, G. J., & Tolchenov, R. N. 2006, *Monthly Notices of the Royal Astronomical Society*, 368, 1087
- Barton, E. J., Hill, C., Yurchenko, S. N., Tennyson, J., Dudaryonok, A. S., & Lavrentieva, N. N. 2017, *Journal of Quantitative Spectroscopy and Radiative Transfer*, 187, 453
- Batalha, N., Domagal-Goldman, S. D., Ramirez, R., & Kasting, J. F. 2015, *Icarus*, 258, 337
- Bell, E. A., Boehnke, P., Harrison, T. M., & Mao, W. L. 2015, *Proceedings of the National Academy of Sciences of the United States of America*, 112, 14518
- Betts, H. C., Puttick, M. N., Clark, J. W., Williams, T. A., Donoghue, P. C. J., & Pisani, D. 2018, *Nature Ecology & Evolution*, 2, 1556
- Dalgarno, A., & Williams, D. A. 1962, *The Astrophysical Journal*, 136, 690
- Ding, F., & Pierrehumbert, R. T. 2016, *The Astrophysical Journal*, 822, 24
- Elkins-Tanton, L. T., & Seager, S. 2008, *The Astrophysical Journal*, 685, 1237
- Fulton, B. J., & Petigura, E. A. 2018, *The Astronomical Journal*, 156, 264
- Genda, H., Iizuka, T., Sasaki, T., Ueno, Y., & Ikoma, M. 2017, *Earth and Planetary Science Letters*, 470, 87
- Giulio, M. D. 2003, *Journal of Theoretical Biology*, 221, 425
- Goldblatt, C. 2015, *Astrobiology*, 15, 362
- Gordon, I. E. et al. 2017, *Journal of Quantitative Spectroscopy and Radiative Transfer*, 203, 3
- Goldblatt, C., Robinson, T. D., Zahnle, K. J., & Crisp, D. 2013, *Nature Geoscience*, 6, 661
- Hamano, K., Abe, Y., & Genda, H. 2013, *Nature*, 497, 607
- Hu, R., Seager, S., & Yung, Y. L. 2015, *The Astrophysical Journal*, 807, 8
- Ingersoll, A. P. 1969, *Journal of the Atmospheric Sciences*, 26, 1191
- Kasting, J. F., Whitmire, D. P., & Reynolds, R. T. 1993, *Icarus*, 101, 108
- Koll, D. D. B., & Cronin, T. W. 2018, *Proceedings of the National Academy of Sciences*, 201809868
- Komabayasi, M. 1967, *Journal of the Meteorological Society of Japan. Ser. II*, 45, 137
- Kopparapu, R. K. et al. 2013, *The Astrophysical Journal*, 765, 131
- Lazcano, A., & Miller, S. L. 1994, *Journal of Molecular Evolution*, 39, 546
- Lebrun, T., Massol, H., Chassefière, E., Davaille, A., Marcq, E., Sarda, P., Leblanc, F., & Brandeis, G. 2013, *Journal of Geophysical Research: Planets*, 118, 1155
- Leconte, J., Forget, F., Charnay, B., Wordsworth, R., & Pottier, A. 2013, *Nature*, 504, 268
- Li, C., & Ingersoll, A. P. 2015, *Nature Geoscience*, 8, 398
- Lopez, E. D., Fortney, J. J., & Miller, N. 2012, *The Astrophysical Journal*, 761, 59
- Luger, R., Barnes, R., Lopez, E., Fortney, J., Jackson, B., & Meadows, V. 2015, *Astrobiology*, 15, 57
- Mlawer, E. J., Payne, V. H., Moncet, J.-L., Delamere, J. S., Alvarado, M. J., & Tobin, D. C. 2012, *Phil. Trans. R. Soc. A*, 370, 2520
- Nakajima, S., Hayashi, Y.-Y., & Abe, Y. 1992, *Journal of the Atmospheric Sciences*, 49, 2256
- Owen, J. E., & Wu, Y. 2016, *The Astrophysical Journal*, 817, 107
- Penz, T., Micela, G., & Lammer, H. 2008, *Astronomy & Astrophysics*, 477, 309
- Pierrehumbert, R. 1995, *Journal of the Atmospheric Sciences*, 52, 1784
- Pierrehumbert, R., & Gaidos, E. 2011, *The Astrophysical Journal*, 734, 1
- Pierrehumbert, R. T. 2010, *Principles of Planetary Climate* (Cambridge, UK: Cambridge University Press)
- Quintana, E. V., Barclay, T., Borucki, W. J., Rowe, J. F., & Chambers, J. E. 2016, *The Astrophysical Journal*, 821, 126
- Rafikov, R. R. 2006, *The Astrophysical Journal*, 648, 666
- Ramirez, R. M., & Kaltenegger, L. 2017, *The Astrophysical Journal Letters*, 837, L4
- Ramirez, R. M., Kopparapu, R., Zuger, M. E., Robinson, T. D., Freedman, R., & Kasting, J. F. 2014, *Nature Geoscience*, 7, 59
- Ribas, I., Guinan, E. F., Güdel, M., & Audard, M. 2005, *The Astrophysical Journal*, 622, 680
- Schaefer, L., & Fegley, B. 2010, *Icarus*, 208, 438
- Segura, A., Krelow, K., Kasting, J. F., Sommerlatt, D., Meadows, V., Crisp, D., Cohen, M., & Mlawer, E. 2003, *Astrobiology*, 3, 689
- Stamnes, K., Tsay, S.-C., Wiscombe, W., & Jayaweera, K. 1988, *Applied Optics*, 27, 2502
- Stevenson, D. J. 1999, *Nature*, 400, 32
- Stockbridge, R. B., Lewis, C. A., Yuan, Y., & Wolfenden, R. 2010, *Proceedings of the National Academy of Sciences*, 107, 22102
- Takai, K. et al. 2008, *Proceedings of the National Academy of Sciences*, 105, 10949
- Voronin, B. A., Lavrentieva, N. N., Mishina, T. P., Chesnokova, T. Y., Barber, M. J., & Tennyson, J. 2010, *Journal of Quantitative Spectroscopy and Radiative Transfer*, 111, 2308
- Walker, J. C. G., Hays, P. B., & Kasting, J. F. 1981, *Journal of Geophysical Research*, 86, 9776
- Wordsworth, R. 2012, *Icarus*, 219, 267
- Wordsworth, R., & Pierrehumbert, R. 2013, *Science*, 339, 64
- Yang, J., Cowan, N. B., & Abbot, D. S. 2013, *The Astrophysical Journal Letters*, 771, L45
- Yang, J. et al. 2016, *The Astrophysical Journal*, 826, 222

A. Escape Timescale of H₂

We first investigate the possibility of direct atmospheric boil-off (Owen & Wu 2016). In this scenario the planet’s atmosphere is so hot and extended that its photosphere (i.e., the altitude at which the atmosphere absorbs the bulk stellar flux) becomes comparable to the planet’s Bondi radius. The atmosphere then undergoes hydrodynamic escape that is powered by the broadband absorbed stellar flux, which allows the planet to shed large amounts of gas over extremely short timescales. To evaluate this possibility we first compute the planet’s Bondi radius,

$$R_b = \frac{GM_p}{2c_s^2}, \quad (38)$$

where M_p is the planet’s mass, $c_s = \sqrt{\tilde{\gamma}kT/m}$ is the speed of sound in H₂, and $\tilde{\gamma} = 1.4$ for a diatomic gas. We compare the Bondi radius to the planet’s photospheric radius. We assume the photosphere is located at 0.1 bar (representative of H₂’s emission level in the infrared; this pressure will be larger at shorter wavelengths so our choice is conservative), and estimate the photospheric radius as

$$R_{photo} = \ln\left(\frac{p_s}{0.1 \text{ bar}}\right) \times H_p, \quad (39)$$

where p_s is the surface pressure and $H_p = kT/(mg)$ is the atmospheric scale height. We find that Earth-sized planets are stable against atmospheric boil-off. For example, even with $T = 1600$ K and $p_s = 1000$ bar, representative of a planet in the late magma ocean stage with a thick H₂ envelope, $R_{photo}/R_b \sim 0.3$.

This leaves hydrodynamic escape powered by the star’s extreme ultraviolet (XUV) flux as the main mechanism capable of eroding an early hydrogen-rich atmosphere (Pierrehumbert & Gaidos 2011; Wordsworth 2012). The escape flux for energy-limited hydrodynamic escape is given by

$$\phi = \frac{\epsilon F_{XUV} R_p}{4GM_p}, \quad (40)$$

where $\epsilon \sim 0.3$ is an efficiency factor, M_p and R_p are the planetary mass and radius, and F_{XUV} is the stellar XUV flux. Our formulation assumes that the main escaping species is atomic hydrogen, i.e., H₂ is photodissociated in the upper atmosphere.

To model the stellar XUV we use the Sun’s current XUV flux at Earth’s orbit in the range $\lambda \leq 0.92 \mu\text{m}$, which is equal to $F_0 = 3.9 \times 10^{-3} \text{ W m}^{-2}$ (Ribas et al. 2005). This excludes Ly α radiation, which does not contribute to the escape flux in the absence of high-altitude absorbers (Pierrehumbert & Gaidos 2011). To bracket the time evolution of the stellar XUV flux we use two different power-laws derived from Solar analogs (Ribas et al. 2005; Penz et al. 2008),

$$F_{XUV} \propto t^{-1.23}. \quad (41)$$

and

$$F_{XUV} \propto \begin{cases} t^{-0.425}, & \text{for } t \leq 0.6 \text{ Gyr}, \\ t^{-1.69}, & \text{for } t > 0.6 \text{ Gyr}. \end{cases} \quad (42)$$

We integrate the escape flux, assuming planet formation ends 100 Myr after the formation of the host star. Figure 7 shows how much H₂ is lost as a function of time, and how these amounts compare to different mechanisms for forming an early H₂-rich atmosphere. We find that thick H₂-envelopes with 70-100 bars of H₂ can be retained over timescales of 60-120 Myr.

B. Validation of Shortwave Radiative Transfer

Figure 8 shows that our code compares favorably against the line-by-line calculations of Goldblatt et al. (2013). To focus on the validity of our radiative transfer we use the same atmospheric temperature and humidity profiles as in Goldblatt et al, and use PyRADS to compute top-of-atmosphere planetary albedos. For reference, other radiative transfer codes produce typical differences of about 1-3% in the top-of-atmosphere planetary albedo for identical atmospheric profiles (Yang et al. 2016). We find that the albedo computed with PyRADS agrees with the results from Goldblatt et al to better than 1%, even though our albedo values are systematically higher.

The remaining small differences in albedo are likely due to different modeling assumptions and the use of different opacity sources. We use the ExoMol BT2 line list, which has a more complete coverage than the line list used by Goldblatt et al, so our computed albedos should be lower in the near-IR and visible. At the same time we only parameterize H₂O absorption in the UV (see Section 2), so we could be underestimating atmospheric absorption at short wavelengths. In addition, we have found that changes in the assumed stellar source function can modify our results by up to several percent, which would be large enough to explain the remaining offset in Figure 8.

⁸ <https://github.com/pcubillos/ApJtemplate>

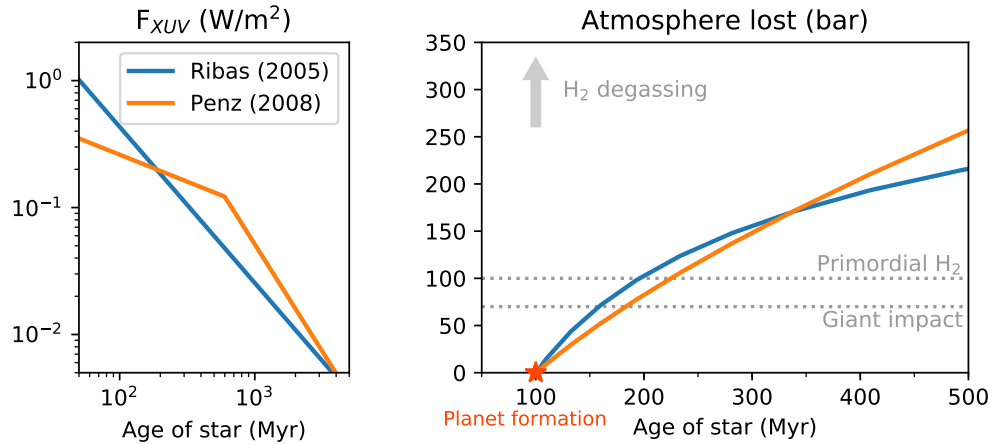


Figure 7. Earth-sized planets can retain thick H₂ envelopes over 100 Myr or longer. Left: XUV fluxes of Sun-like stars at 1 AU. Right: Atmospheric hydrogen lost for each XUV scaling. Grey lines and grey arrow indicate different three mechanisms for generating a H₂ atmosphere: outgassing from a magma ocean (Elkins-Tanton & Seager 2008), gravitational capture of primordial H₂ (Pierrehumbert & Gaidos 2011), and oxidation of iron in reaccreting giant-impact fragments (Genda et al. 2017).

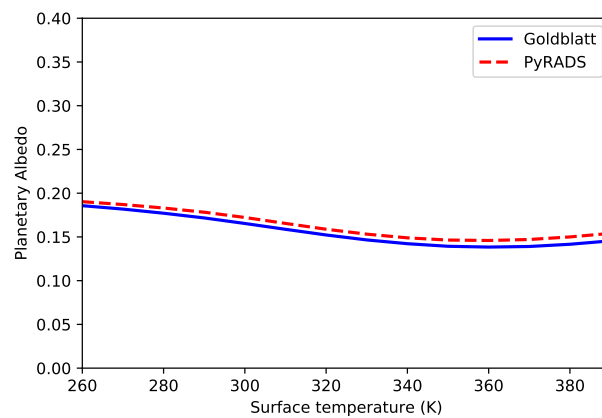


Figure 8. Validation of our shortwave calculations. Solid line show planetary albedo from a reference set of line-by-line calculations (Goldblatt et al. 2013), dashed line shows our results. All calculations are performed with a surface albedo of 0.12 and 1 bar of N₂.